Focusing properties of surface plasmon polariton floating dielectric lenses

Hwi Kim, Joonku Hahn, and Byoungho Lee*

National Creative Research Center for Active Plasmonics Application Systems,
Inter-University Semiconductor Research Center and School of Electrical Engineering,
Seoul National University, Seoul 151-744, Korea
[*]Corresponding author: byoungho@snu.ac.kr

http://oeqelab.snu.ac.kr

Abstract: We have investigated the focusing properties of surface plasmon polariton floating dielectric lenses. An analysis of the scattering characteristics of surface plasmon polaritons using a floating dielectric block shows that the air-gap thickness between a floating dielectric block and a metal substrate can be an effective dynamic variable for modulating the amplitude and phase of the transmission coefficient of the surface plasmon polaritons. This property can be used to realize a variable-focusing surface plasmon dielectric lens with the air-gap thickness as the dynamic variable. The focusing properties of a Fresnel lens and a parabolic lens with respect to the air-gap thickness are compared and analyzed.

OCIS codes: (240.6680) Surface plasmons; (250.5300) Photonic integrated circuits

References and links

1. W. L. Barnes, A. Dereux, and T. W. Ebbesen, "Surface plasmon subwavelength optics," Nature **424**, 824-830 (2003).
2. P. Berini, R. Charbonneau, and N. Lahoud, "Long-range surface plasmons on ultrathin membranes," Nano Lett. **7**, 1376-1380 (2007).
3. I.-M. Lee, J. Jung, J. Park, H. Kim, and B. Lee, "Dispersion characteristics of channel plasmon polariton waveguides with step-trench-type grooves," Opt. Express **15**, 16596-16603 (2007).
4. J. Takahara and T. Kobayashi, "Low-dimensional optical waves and nano-optical circuits," Opt. Photon. News **15**, 54-59 (2004).
5. S. Kim, H. Kim, Y. Lim, and B. Lee, "Off-axis directional beaming of optical field diffracted by a single subwavelength metal slit with asymmetric dielectric structure surface gratings," Appl. Phys. Lett. **90**, 051113 (2007).
6. S. Kim, Y. Lim, H. Kim, J. Park, and B. Lee, "Optical beam focusing by a single subwavelength metal slit surrounded by chirped dielectric surface gratings," Appl. Phys. Lett. **92**, 013103 (2008).
7. I. P. Radko, S. I. Bozhevolnyi, A. B. Evlyukhin, and A. Boltasseva, "Surface plasmon polariton beam focusing with parabolic nanoparticle chains," Opt. Express **15**, 6576-6582 (2007).
8. W. Nomura, M. Ohtsu, and T. Yatsui, "Nanodot coupler with a surface plasmon polariton condenser for optical far/bear-field conversion," Appl. Phys. Lett. **86**, 181108 (2005).
9. R. Zia and M. L. Brongersma, "Surface plasmon polariton analogue to Young's double-slit experiment," Nature Nanotech. **2**, 426-429 (2007).
10. F. Lopez-Tejeria, S. G. Rodrigo, L. Martin-Moreno, F. J. Garcia-Vidal, E. Devaux, T. W. Ebbesen, J. R. Krenn, I. P. Padko, S. I. Bozhevolnyi, M. U. Gonzalez, J. C. Weeber, and A. Dereux, "Efficient unidirectional nanoslit couplers for surface plasmons," Nature Phys. **3**, 324-328 (2007).
11. P. Lalanne and E. Silberstein, "Fourier-modal methods applied to waveguide computational problems," Opt. Lett. **25**, 1092-1094 (2000).
12. H. Kim, I.-M. Lee, and B. Lee, "Extended scattering-matrix method for efficient full parallel implementation of rigorous coupled-wave analysis," J. Opt. Soc. Am A **24**, 2313-2327 (2007).
13. J. W. Goodman, Introduction to Fourier Optics, 3rd ed., (Roberts & Company Publishers, Englewood, 2005).

#91595 - $15.00 USD Received 10 Jan 2008; revised 15 Feb 2008; accepted 15 Feb 2008; published 20 Feb 2008

1. Introduction

Optical information processing on the nano-scale is considered to be a main objective in the field of nanophotonics. Recently, optical information processing on the nano-scale has become a reality because of the exploitation of the full potential of surface plasmon polaritons (SPPs) [1-3]. An SPP is a low-dimensional electron-electromagnetic coupled surface wave that usually exists at a metal/dielectric interface [4]. As a basic control mechanism of SPP, the diffraction of SPP by a nanostructure is one of the most important topics related to SPPs and their applications.

In contrast to radiational diffraction of SPPs, such as beaming [5, 6], low-dimensional diffraction of SPPs means that the diffracted field of the SPP is still a low-dimensional wave confined at the metal/dielectric interface, even though, from the surface diffractive structures, part of the optical energy can radiate into the surrounds. Plasmonic information processing assumes that most information processing is performed at the metal/dielectric interfaces that sustain SPPs. Devices for plasmonic information processing need to be designed for the low-dimensional diffraction of SPP.

There has been research into the low-dimensional diffraction of SPPs and their applications. Several parabolic lens structures for SPPs have been demonstrated [7, 8]. Recently, a double slit experiment of SPPs [9] was reported to show that the low-dimensional diffraction theory analogue to Fresnel diffraction theory is applicable to SPPs. Plasmonic bandgap structures [10] are also based on the low-dimensional diffraction of SPPs. Other functions for SPPs that correspond to well-known optical functions in conventional optical information processing are being developed continuously.

In this paper, we consider an SPP dielectric lens that is one of the basic devices for plasmonic information processing. In particular, we address the variable-focusing properties of SPP floating dielectric lenses. For this purpose, we aimed to find a potential dynamic structural variable that could control the focusing of an SPP lens. In this paper, an analysis on the scattering characteristics of SPPs using a floating dielectric block was performed employing rigorous coupled wave analysis (RCWA) [11, 12]. In the focusing of an SPP through a lens structure, the scalar diffraction theory with an angular spectrum representation [9] was adopted to describe the field propagation of an SPP modulated by a lens structure.

In Section 2, the modulation characteristics of SPP eigenmode by a finite-size dielectric block floating over a metal substrate are analyzed using RCWA. In Section 3, the focusing properties of an SPP floating dielectric lens are discussed using scalar diffraction theory, and in Section 4, concluding remarks are given.

2. Modulation of surface plasmon polariton eigenmode using a finite-size dielectric block floating over a metal substrate

Figure 1 shows a schematic drawing of the structure investigated and the SPP diffraction. The finite-size dielectric block floats over a metal substrate, and the air/metal interface can hold an SPP eigenmode. The SPP eigenmode is scattered by the floating dielectric block. The length of the dielectric block and the air-gap thickness between the dielectric block and the metal substrate are denoted by t and h, respectively. The length, t, is a fixed structural parameter that cannot be controlled dynamically, while the air-gap, h, is an effective dynamic structural variable that can be controlled using highly developed nano-scale actuators.

In this section, using RCWA, we investigate the scattering characteristics of the SPP eigenmode passing through the region of a finite-size dielectric block floating over a metal substrate. We assume that the wavelength of the optical field is 632.8nm and, at this wavelength, the permittivity values of a metallic (Au) substrate, air, and dielectric block are $\varepsilon_m(=-9.5487+j1.1327)$, $\varepsilon_{\mathrm{a}}(=1)$, and $\varepsilon_{\mathrm{b}}(=2.25)$, respectively.

To use the RCWA, let the SPP eigenmode of the air/metal interface propagating along the z-direction be denoted by $E^{+}_{n_{spp}}(x,y,z)$, where n_{spp} is the mode index of the SPP eigenmode in the RCWA scheme, and the superscript $+$ denotes the positive z-directional propagation of the SPP eigenmode. In the modal analysis framework of the RCWA [11, 12], the reflection field (Region I) and the transmission field (Region II) are represented as linear combinations of the eigenmodes $E_n^{\pm}(x,y,z)$ with coupling coefficients, $C_n^{\pm}$,

$$E_R = \sum_n C_n^- E_n^-(x,y,z) \qquad \text{for} \quad z<0, \tag{1a}$$

$$E_T = C_{n_{spp}}^+ E_{n_{spp}}^+(x,y,z-t) + \sum_{n \neq n_{spp}} C_n^+ E_n^+(x,y,z-t) \qquad \text{for } z>t. \tag{1b}$$

In the RCWA, the permittivity profile over the entire space is represented by a Fourier series, and the Maxwell equations are described as a linear eigenvalue equation in the spatial-frequency domain. In this framework, the pseudo-Fourier series coefficients of the eigenmodes, $E_n^{\pm}(x,y,z)$, are the eigenvectors of the linear eigenvalue equation. The coupling coefficients, $C_n^{\pm}$, are determined by the mode matching (boundary) conditions at $z=0$ and $z=t$. When solving the mode matching conditions, we can excite the SPP eigenmodes selectively in Region I, as indicated in Fig. 1. In the analysis of the low-dimensional diffraction of SPPs, we only need to consider the SPP mode in Region II, $C_{n_{spp}}^+ E_{n_{spp}}^+(x,y,z-t)$, in Eq. (1b). The second term in Eq. (1b), $\sum_{n \neq n_{spp}} C_n^+ E_n^+(x,y,z-t)$, indicates the sum of the radiating and highly evanescent modes that cannot actually propagate along the *z*-direction. The transmission coefficient, $C_{n_{spp}}^+$, is the key factor in the analysis. The amplitude and phase of $C_{n_{spp}}^+$ is interpreted as the amplitude and phase modulation value of the incident SPP eigenmode. The floating dielectric block modulates the SPP eigenmode when the air-gap thickness is within a reasonable range wherein an evanescence tail of an SPP eigenmode can touch the dielectric block. When the air-gap thickness is large enough to be out of this range, the SPP eigenmode is not perturbed by the dielectric block, since the evanescence tail has a finite length along the *x*-direction.

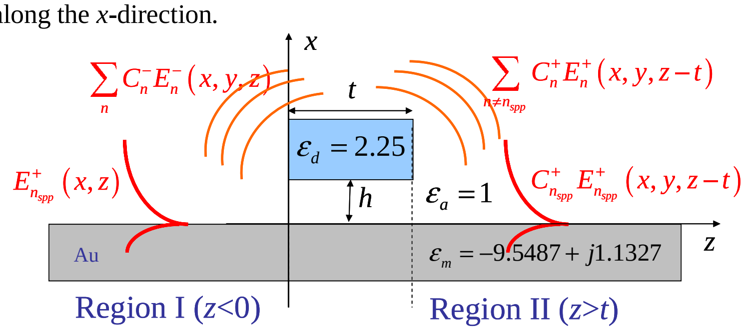

Fig. 1. Scattering of surface plasmon polariton eigenmode by a finite size dielectric block

Using RCWA, we calculate the transmission coefficients for various lengths and air-gap thicknesses, where a perfectly matched layer (PML) is adopted for an aperiodic structure analysis [5, 6]. The total number of *x*-direction Fourier spatial harmonics is set to 61, which is the number of spatial harmonics showing a reasonable convergence, and the *x*-direction supercell periods, L_x, is chosen to be $7\mu m$. Figures 2 and 3 show the distribution of the

#91595 - $15.00 USD Received 10 Jan 2008; revised 15 Feb 2008; accepted 15 Feb 2008; published 20 Feb 2008

transmission coefficient, $C^+_{n_{spp}}$, for two dielectric blocks with thicknesses along the *x*-direction of $1\mu m$ and $2\mu m$, respectively.

To better understand these distributions, the electric field distribution for these specific cases is presented for each case. Let us consider the case of a dielectric block with a thickness of $1\mu m$. Figures 2(a) and 2(b) show the amplitude, $\left|C^+_{n_{spp}}\right|$, and the phase, $\measuredangle C^+_{n_{spp}}$, distributions of $C^+_{n_{spp}}$ for changes in the length, t, from $0\mu m$ to $10\mu m$ and the air-gap thickness, h, from $0\mu m$ to $0.5\mu m$. Within the air-gap region below $50nm$, we can observe a trend that as the length increases, the amplitude of the transmission coefficient decreases monotonically because of ohmic loss and radiation loss. However, in the air-gap region above $50nm$, a complex amplitude fluctuation along the length axis is observed. This amplitude fluctuation originates from the finite thickness of the dielectric block. This point can be visually understood by comparing Figs. 2(c) and 2(d). These figures show the *x*-polarization and *z*-polarization electric field distributions of the cases where the air-gap thickness of 0 and 150nm, respectively. In the latter case, due to the air-gap, the radiation into the dielectric block is significant, but the radiation field immediately becomes a guided multimode of the dielectric block because of the total internal reflection (TIR), as seen in Fig. 2(d). The wave bundle reflected by the ceiling of the dielectric block transfers some optical energy to the SPP eigenmode. Thus, we can observe a periodic amplitude fluctuation along the length axis in the air-gap region above a distance of $50nm$. In addition, as shown in Fig. 2(b), we can observe a more sensitive change in the phase-varying rate along the length axis compared to the variation in air-gap thickness, and the phase-varying rate is lowered in the air-gap range above 50nm.

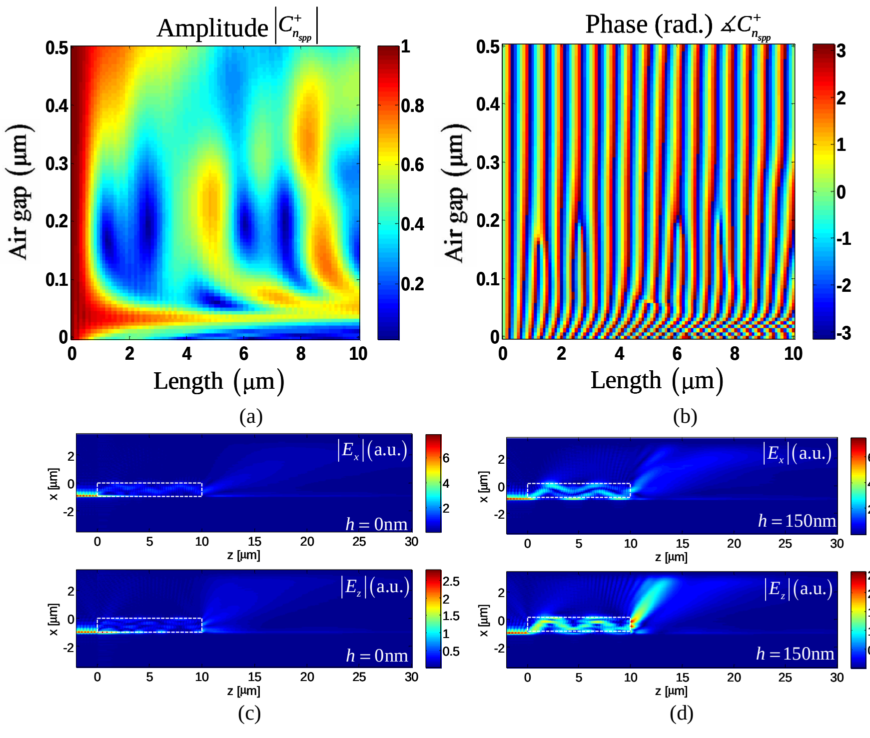

Fig. 2. (a) Amplitude modulation profile and (b) phase modulation profile with respect to the air-gap thickness, *h*, and length, *t*. Here, the thickness of the dielectric block is $1\mu m$. (c) *x*-polarization and *z*-polarization electric field distributions in the case of an air-gap thickness of 0nm. (d) *x*-polarization and *z*-polarization electric field distribution in the case of an air-gap thickness of 150nm.

#91595 - $15.00 USD Received 10 Jan 2008; revised 15 Feb 2008; accepted 15 Feb 2008; published 20 Feb 2008

For comparison, the distribution of the transmission coefficient, $C^{+}_{n_{spp}}$, in the case of a dielectric block with a thickness of $2\mu m$ is shown in Fig. 3. In the same way as the dielectric block with a thickness of $1\mu m$, it can be seen that as the length increases, the amplitude of the transmission coefficient decreases monotonically because of ohmic loss and radiation loss when the air-gap is smaller than 50nm.

From Figs. 2 and 3, it is noted that the amplitude and phase distribution profiles of a dielectric block with a thickness of $2\mu m$ is almost similar to those of a dielectric block with a thickness of $1\mu m$. The SPP modulation profile is not sensitive to the thickness of the dielectric block, since below an air-gap thickness of 50nm, the surface bound mode plays a dominant role in transferring optical energy through the dielectric block region. The transmission properties for an air-gap thickness around $50nm$, as shown in Figs. 2 and 3, are very interesting. A resonant high transmission feature is observed, which can be exploited for high efficient SPP devices. Periodic amplitude fluctuations along the length axis are observed in the air-gap region above 50nm. In this case, because the thickness of the dielectric block is double that of the former case, the fluctuation period is also doubled.

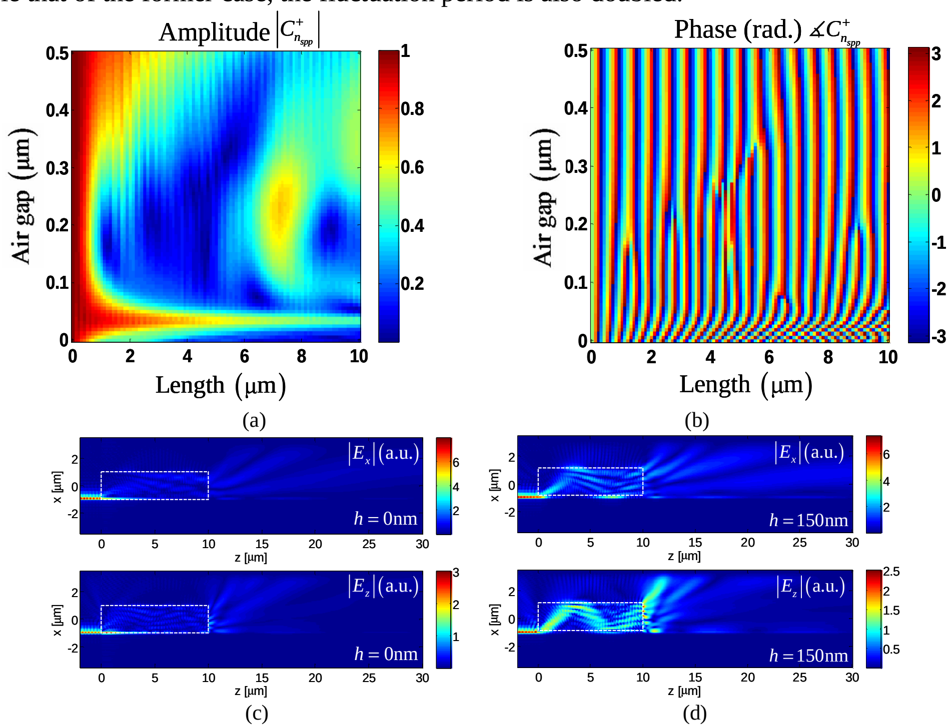

Fig. 3. (a) Amplitude modulation profile, and (b) phase modulation profile with respect to air-gap thickness, *h*, and length, *t*. Here, the thickness of the dielectric block is $2\mu m$. (c) *x*-polarization and *z*-polarization electric field distribution in the case of an air-gap thickness of 0nm. (d) *x*-polarization and *z*-polarization electric field distributions in the case of an air-gap thickness of 150nm.

The modulation features discussed originate from the mixed effect of radiational coupling between the SPP eigenmode and the dielectric block, scattering at the boundary of the finite-size dielectric block, and the internal mode structure of the air/dielectric/air/metal structure. An exact understanding of these modulation properties requires a further investigation involving deep modal analysis. We are preparing a paper on the interesting high-transmission feature through a floating dielectric block with an air-gap thickness around 50nm. In this

#91595 - $15.00 USD Received 10 Jan 2008; revised 15 Feb 2008; accepted 15 Feb 2008; published 20 Feb 2008

paper, we present a possible application of this modulation property, which is described in the next section.

By using a numerical polynomial fitting method, we can finally obtain a polynomial-represented functional relationship,

$$C^{+}_{n_{spp}}\left(h,t\right)=A\left(h,t\right)\exp\left(j\Phi\left(h,t\right)\right), \tag{2}$$

which is parameterized by an air-gap, h, and length, t. The real coefficient polynomial fitting functions of the amplitude and phase distribution are given by $A(h,t)$ and $\Phi(h,t)$, respectively. In particular, the phase fitting function, $\Phi(h,t)$, is a polynomial that approximates the unwrapped phase profile.

3. Focusing properties of surface plasmon polariton floating dielectric lenses

In this section, the focusing properties of SPP floating dielectric lenses are discussed, based on the scattering analysis described in the previous section. Figure 4 shows a schematic drawing of an SPP focused using a floating parabolic dielectric lens. For the description of the lens transmittance, we adopt the thin element approximation in scalar Fourier optics [13].

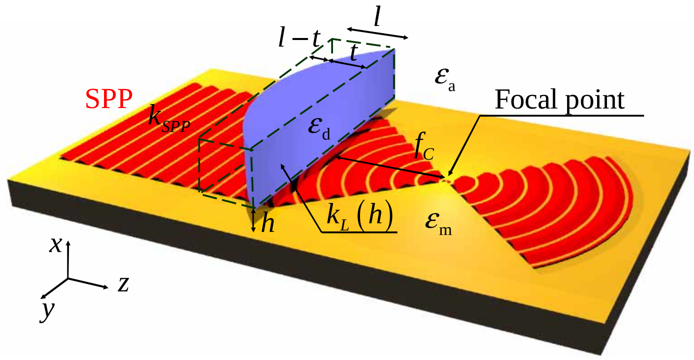

Fig. 4. Surface plasmon polariton focusing using a floating dielectric lens.

A lens profile that makes a spherically converging wavefront can be obtained from Eq. (2). The phase and amplitude modulations by the lens at a specific position y, $\phi(h,y)$ and $\Gamma(h,y)$, respectively, are given by,

$$\phi(h,y)=\Phi\left(h,t(y)\right)-k_{spp}t(y), \tag{3a}$$

$$\Gamma(h,y)=A_{spp}\left(l-t(y)\right)A\left(h,t(y)\right), \tag{3b}$$

where k_{spp} is the wavenumber of the SPP eigenmode, $A_{spp}(s)$ is the modal amplitude of the SPP eigenmode that is propagated a distance, s, $t(y)$ is the lens surface profile function, and l is the maximum longitudinal thickness of the lens, as shown in Fig. 4.

For comparison, a parabolic lens and a Fresnel lens with 2π modulo are considered. The lens profile function, $t(y)$, for changing the incident SPP eigenmode to a spherically converging SPP wave was designed using the following procedure. The profile function,

$t(y)$, of a parabolic lens and a Fresnel lens that produce the same spherical wavefront, needs to satisfy the polynomial Eqs. (4a) and (4b), respectively,

$$\Phi(h,t(y)) - \mathrm{Re}(k_{spp})t(y) = \mathrm{Re}(k_{spp})\left(\sqrt{f_c^2 + y_{\max}^2} - \sqrt{f_c^2 + y^2}\right), \tag{4a}$$

$$\begin{aligned}&\Phi(h,t(y)) - \mathrm{Re}(k_{spp})t(y)\\&= \mathrm{Re}(k_{spp})\left(\sqrt{f_c^2 + y_{\max}^2} - \sqrt{f_c^2 + y^2}\right) - 2\pi\left[\mathrm{Re}(k_{spp})\left(\sqrt{f_c^2 + y_{\max}^2} - \sqrt{f_c^2 + y^2}\right)/(2\pi)\right],\end{aligned} \tag{4b}$$

where y is limited to the range $-y_{\max} \le y \le y_{\max}$, $[\cdot]$ is Gauss' symbol, $\mathrm{Re}(s)$ is the real part of a complex number s, and f_c is the focal length of the lens. We can easily find the value of $t(y)$ by using standard numerical root-finding libraries. The incident SPP eigenmode is transformed to the SPP mode with a spherically converged wavefront, $\Gamma(h,y)\exp(j\phi(h,y))$, for $-y_{\max} \le y \le y_{\max}$, and at the flat facet of the lens.

We used the angular spectrum representation [9, 13] to simulate the wave propagation. Let us denote the angular spectrum of the modulated wavefront profile at the flat facet by $\Pi(\alpha;h)$. Then, $\Pi(\alpha;h)$ is obtained as,

$$\Pi(\alpha;h) = \int_{-\infty}^{\infty} \Gamma(h,y)\exp(j\phi(h,y))\exp(-j2\pi\alpha y)\,dy, \tag{5a}$$

where α is the *y*-direction spatial-frequency component. Using the angular spectrum propagation formula [13], the SPP field distribution at the air/metal interface $(x=0)$ can be approximated as,

$$E(y,z;h) = \int_{-\infty}^{\infty} \Pi(\alpha;h)\exp(j2\pi\alpha y)\exp\left(j\sqrt{(k_{spp})^2 - (2\pi\alpha)^2}\,z\right)d\alpha, \text{ for } z > 0. \tag{5b}$$

The transmission efficiency, T_e, is the ratio of transmission power to the input power, defined by,

$$T_e = 100 \times \int_{-\infty}^{\infty} \left|\Pi(\alpha;h)\right|^2 \mathrm{Re}\left(\sqrt{(k_{spp})^2 - (2\pi\alpha)^2}\right)/\mathrm{Re}(k_{spp})\,d\alpha\,(\%). \tag{6}$$

The focusing properties of the parabolic and Fresnel lens are compared with the above described simulation method. Both the parabolic lens and the Fresnel lens are designed with an air-gap thickness of 50nm. As the air-gap thickness decreases monotonically below 50nm, the amplitude and phase modulation profiles are changed according to Eqs. (3a) and (3b). The lens thickness is assumed to be $2\mu\mathrm{m}$ (see Fig. 3).

Figure 5 shows the SPP field distributions obtained for several cases with changes in air-gap thickness. The air-gap thickness is changed from 0 to 50nm. Figures 5(a) and 5(b) show the focusing properties of a parabolic lens and a 2π modulo Fresnel lens, respectively, with the same focal length of $10\mu\mathrm{m}$. Figures 5(c) and 5(d) show the focusing properties of a

#91595 - $15.00 USD Received 10 Jan 2008; revised 15 Feb 2008; accepted 15 Feb 2008; published 20 Feb 2008

parabolic lens and a Fresnel lens, respectively, with the same focal length of 5μm . The transmission efficiency, T_e , of each lens is also shown in Fig. 5.

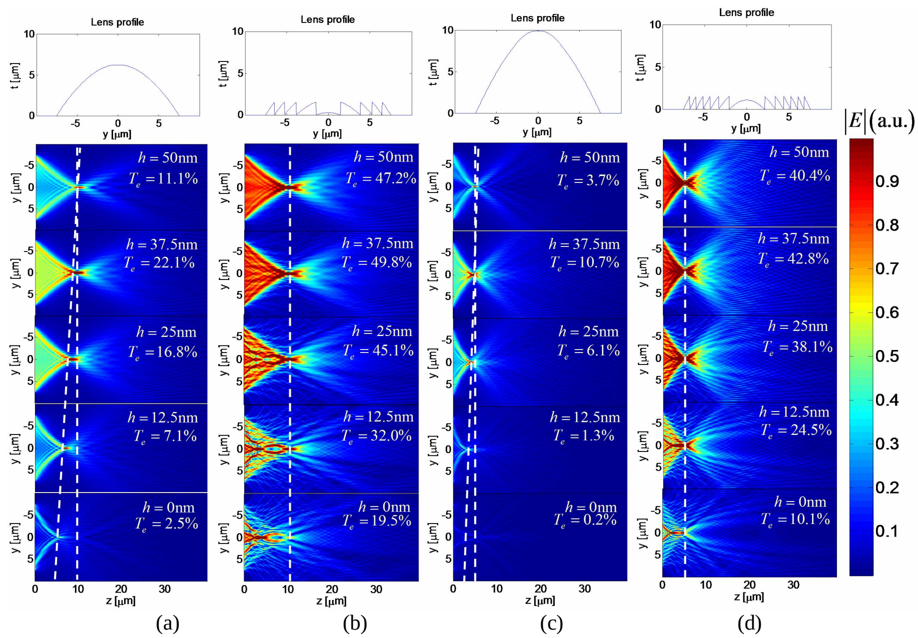

Fig. 5. (a) Focusing using a floating parabolic lens with a focal length of 10μm , (b) focusing using a floating Fresnel lens with a focal length of 10μm , (c) focusing using a floating parabolic lens with a focal length of 5μm , and (d) focusing using a floating Fresnel lens with a focal length of 5μm .

As shown in the simulation results, a linear change in the air-gap thickness, decreasing from 50 to 0nm, gives a decrease in the linear focal length to half the focal length in the case of the floating parabolic lens, while change in focal length is not observed in the case of the floating Fresnel lens. In the Fresnel lens structure, the focusing profile deteriorates without a change in focal length. The focal length of the Fresnel lens is less influenced by changes in air-gap, i.e., a change in the effective refractive index, since the focal length is mainly determined by the spatial diffractive profile, which is fixed. As the focal length becomes shorter, the thickness of the parabolic lens increases and the transmission amplitude decreases because of radiation loss.

Thus, at the matched air-gap of 50nm, the relatively thin Fresnel lens structure has superior transmission efficiency to the relatively thick parabolic lens structure. However, we can only obtain a dynamic variable-focusing property using parabolic lens structures.

4. Conclusion

In conclusion, we have shown that an air-gap control of a floating dielectric block can generate the dynamic phase and amplitude modulation of the SPP transmission coefficient. As an application of this property, we have demonstrated the variable-focusing properties of an SPP floating dielectric parabolic lens using numerical simulations and compared the focusing properties of SPP parabolic lenses and SPP Fresnel lenses. Unlike conventional bulk optics, the nano-scale surface optics for SPP processing contains several unexpected and interesting features in addition to the physical features described in this paper. Dynamic plasmonic information processing on the nano-scale using air-gap control may be an effective mechanism for building a dynamic plasmonic information processing system. In this paper,

#91595 - $15.00 USD Received 10 Jan 2008; revised 15 Feb 2008; accepted 15 Feb 2008; published 20 Feb 2008

we have shown that the air-gap range showing a linear modulation properties for a wavelength of 632.8nm is 0~50nm. However, for longer wavelengths such as telecommunication wavelengths or terahertz wavelengths, the air-gap dynamic range showing linear modulation characteristics may be broader. In this case, the idea of controlling the air-gap will become more feasible in practice. The modulation structures of an SPP using floating dielectric structures as investigated may be exploited in several SPP-based applications, such as SPP diffractive optical elements and SPP integrated circuit devices.

Acknowledgment

The authors acknowledge the support of the Ministry of Science and Technology of Korea and the Korea Science and Engineering Foundation through the Creative Research Initiative Program (Active Plasmonics Application Systems).

#91595 - $15.00 USD Received 10 Jan 2008; revised 15 Feb 2008; accepted 15 Feb 2008; published 20 Feb 2008